Electronic Letters on Computer Vision and Image Analysis 25(1):22-42, 2025

Optimized Deep Learning Architecture for Melanoma Detection: Leveraging ResNet50V2.5 in Dermatological Imaging

S. Shafeena*, Vinod Kumar. R. S#, Kumar S S$ and Shahi D@

* *Ph.D Research Scholar,* # *Professor,* $ *Associate Professor,* @ *Assistant Professor*
* # @ *Department of Electronics and Communication Engineering,*
$ *Department of Electronics and Instrumentation Engineering,*
* # $ @ *Noorul Islam Centre for Higher Education, Kumaracoil, Tamil Nadu, India*

Received 14th of July 2025; Accepted 06th of March 2026

Abstract

Melanoma is one of the most aggressive types of skin cancer and significantly contributes to the global mortality associated with skin malignancies. Accurate detection and precise assessment of disease severity are critical for enhancing patient survival and treatment outcomes. However, the automatic classification of skin lesions from images remains a challenging task due to subtle and complex variations in their visual features. This study describes deep learning techniques for effectively distinguishing between benign and malignant melanoma skin cancers. The malignancies are categorized into seven distinct types, namely, melanoma, melanocytic nevus, basal cell carcinoma, actinic keratosis, benign keratosis, dermatofibroma, and vascular lesion. The initial phase of the proposed system involves a preprocessing pipeline incorporating normalization and data augmentation strategies to prepare the HAM10000 dataset for accurate classification. A novel deep learning architecture, ResNet50V2.5, a modified version of the Residual Neural Network, is introduced to improve image classification by removing redundant layers and enhancing training efficiency. A comparative evaluation of five network models, ResNet101, ResNet101V2, ResNet50, ResNet50V2, and the proposed ResNet50V2.5, reveals that ResNet50V2.5 achieves the highest accuracy, reaching a classification performance of 99.17%, thus outperforming existing architectures in skin cancer diagnosis. The practical implications of this work suggest that the proposed model can assist dermatologists in making more reliable and timely diagnoses, thereby improving clinical decision-making in healthcare. Furthermore, future research should explore integrating multimodal medical data, explainable AI techniques, and real-time deployment strategies to enhance the clinical applicability and robustness of these models.

Key Words: Melanoma, ResNet, Deep Learning Algorithms, Pre-processing, Classification, Lesions

The complete training and evaluation code is given in `https://github.com/shafeena90/custom_resnet_melanoma.git`

Correspondence to: inform2shafeena@gmail.com

Recommended for acceptance by Angel D. Sappa
https://doi.org/10.5565/rev/elcvia.2271
ELCVIA ISSN: 15108-5097
Published by Computer Vision Center / Universitat Autonoma de Barcelona, Barcelona, Spain

1 Introduction

Melanoma is one type of skin cancer that presents a significant public health burden globally, with 2 to 3 million new cases per year diagnosed throughout the world [1]. The contrary phenomenon is the higher incidence of skin cancer in dark-skinned individuals, though it is generally associated with whites. Nonmelanoma skin cancer, such as basal cell carcinoma and squamous cell carcinoma, remains the most common type in India, but the composition of the melanoma burden is also on the rise in India. Cancers of the skin contribute 1 to 2% of India's cancer load with tremendous interregional variation. While melanoma incidence rates in northern India were 1.62 per 100,000 males and 1.21 per 100,000 females, non-melanoma skin cancers were the most common in the east and northeast with rates of 6.2/100,000 males and 3.49/100,000 females [2]. Although its lower prevalence compared to other cancers, the high mortality rate of melanoma highlights the need for early, reliable diagnosis.

Diagnosing skin lesions is a challenging task due to visual similarity between classes, complex pattern structures, and subjectivity in manual analysis, leading to misclassification and other issues in the process [3]. The solution to these challenges is the partitioning of cutaneous lesions into seven clinically relevant classes: dermatofibroma, actinic keratosis, benign keratosis, basal cell carcinoma, melanoma, melanocytic nevus, and vascular lesion, as depicted in Figure 1. Furthermore, automated image analysis and deep learning approaches have increasingly been recognized as potent means of aiding the early and accurate diagnosis of melanoma.

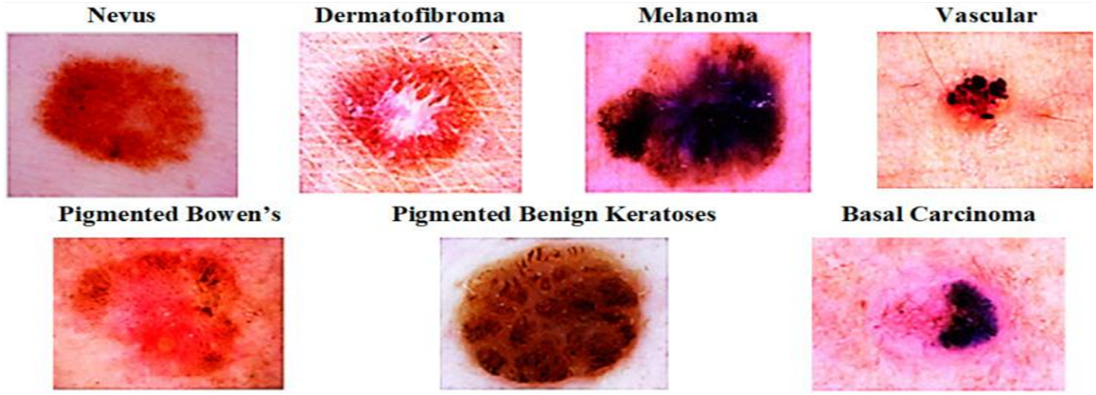

Figure 1: Samples of Skin disease categories from International Skin Imaging Collaboration (ISIC) dataset [4]

The purpose of the research is to assess and improve the automatic classification of skin lesions using ResNet architectures. Specifically, it analyzes the performance of ResNet50, ResNet101, ResNet101V2, ResNet50V2 and the newly introduced ResNet50V2.5 meta-model on the HAM10000 dataset. ResNet50V2.5 architecture includes structural modifications for facilitating gradient flow, enhancing feature representation, and stabilizing training, and is therefore more capable of handling imbalanced skin lesion data.

This proposed research has the potential to provide dermatologists with an effective, reliable, and automated diagnostic aid that can significantly reduce inter-observer variation, expedite the decision-making process, and potentially improve patient clinical outcomes by detecting lesions that the human eye would miss. Meanwhile, it also recognizes some limitations, especially the reliance on the HAM10000 dataset, which may limit generalizability to wider clinical practice. To be robust, the study performs an extensive analysis considering accuracy, precision, recall, F1-score, MCC, Cohens Kappa, Hamming Loss and Jaccard Score. The key novelty of this work comes from ResNet50V2.5, which incorporates a new residual stage, improved bottleneck structures, and a better training strategy, boosting classification accuracy. By systematically comparing different ResNet modifications and demonstrating the superior performance of the altered architecture, this work demonstrates that deep learning has tremendous potential to revolutionise the dermatologic diagnosis of skin cancer. These results are hoped to facilitate subsequent research in areas including explainable AI methods, multimodal data fusion, and ultimately, the translation of the model into clinical decision-support systems.

This section provides a quick overview of the various forms of skin cancer. While Section 2 discusses related work in skin cancer, Section 3 focuses on the materials and methods used in this paper. Section 4 presents the detailed experimental design and its findings. Section 5 summarises the Conclusion.

2 Related Works

The diagnosis of skin cancer is a well-studied problem where focus is given on finding highly accurate and efficient systems. Early diagnosis can reduce mortality to 90% [5], enabling minimally invasive treatment and a good recovery [6]. Image computing techniques using non-invasive sampling can be cost-effective diagnostic aids for lesion monitoring and training [7].

The use of Artificial Intelligence (AI) in medicine has become paramount, and multiple applications in dermatology have been reported, allowing autonomous detection and treatment of skin conditions [8, 9]. Automatic diagnosis methods show a sensitivity of 95% and a specificity of around 90%, performing close to that of dermatologists [10] [11]. Supervised [12], semi-supervised [13], and unsupervised [14] learning are among the machine learning (ML) tools in AI. Cancer prediction is commonly performed by applying supervised learning and deep learning frameworks, such as ANNs [15, 16], CNNs [18], DNNs [17], LSTMs [19], and RNNs [20], which have been prevalently adopted in clinical medicine for cancer detection. Positron emission tomography (PET)[65], most commonly performed as FDG-PET/CT, is a highly effective imaging technique for staging, identifying distant metastases, and monitoring treatment response in high-risk cutaneous melanoma patients.

There are many works on the detection and image classification of skin cancer [20, 21, 22]. Conventional classifiers include, for example, decision trees [23, 24], Bayesian models [25, 26], and SVMs [22, 27], which were later enhanced by AI-based methods [28, 29]. CNNs, first proposed by Fukushima [30] and further developed by LeCun [31], revolutionized image classification via modelling Human visual perception. For example, Esteva et al. [32] used 129,450 images with the GoogLeNet Inception V3 model, achieving 72.1% accuracy. Yu et al. [33] employed a 50-layer CNN model and reached an accuracy of 85.5%. Dorj et al. [34] combined Error-Correcting Output Codes (ECOC) SVM with AlexNet, achieving an accuracy of 95.1%. Han et al. [35] used CNNs to classify 12 types of dermoscopic diseases, achieving 96% accuracy.

Hybrid models provided an advanced performance. Roffman et al. [36] combined an ANN with health-related factors such as age, BMI, and lifestyle to enhance melanoma detection (non-melanoma skin lesions). Murugan et al. [37] integrated SVM with RF for feature identification and obtained better performance than individual learning machines. Tembhurne et al. [38] introduced a hybrid ML-DL method achieving 93% accuracy, surpassing dermatologists' accuracy. Vidya et al. [39] used ABCD, GLCM, and HOG with ML-based classifiers and achieved the best result with SVM, achieving an accuracy of 97.8%. Tumpa and Kabir [40] and Yuhandri et al. [41] achieved strong results on smaller datasets, and Kumar et al. [42] designed an ANN-DE-based mobile approach yielding 97.4% accuracy.

Recent CNN-based methods demonstrate excellent results on HAM10000 and PH2 data sets. This method was well executed by Nawaz et al. [43]. Raja Subramanian et al. [44] developed a CNN model using the HAM10000 dataset, achieving over 80% accuracy, more than 80% precision, and a false-negative rate below 10%, demonstrating CNNs' strong ability to classify skin cancer from dermatoscopic images. Rezaonana et al. [45] proposed an automated method using deep CNNs with transfer learning and image segmentation, achieving 79.45% accuracy in classifying nine types of skin cancer, including melanoma and basal cell carcinoma. Gouda and Amudha [46] showed that a ResNet model reached 92% accuracy in detecting skin lesions, highlighting its potential for early diagnosis. Arief et al. [47] tested various ResNet variants, achieving a validation accuracy of 0.83 and an F1 score of 0.46. Mehra et al. [48] achieved an accuracy of 98.8% by stacking a ResNet50 model with an SVM.

The ResNet architectures proposed by He et al. [49] include residual blocks that alleviate the vanishing gradient problem [50] and thus enable deeper, more effective models. ResNet50, ResNet101, and ResNet152, which differ mainly in depth, also exhibit strong classification performance. ResNet50, ResNet101, ResNet101V2, ResNet50V2, and ResNet50V2.5 are evaluated on HAM10000 for the classification of melanoma.

3 Materials and Methods

3.1 Dataset

The HAM10000 [51] dataset is a widely used benchmark dataset for skin lesion analysis and skin cancer classification. It consists of 10,015 dermoscopic images collected from different clinical sources and populations, ensuring diversity in lesion appearance. All images are provided in RGB color format with a resized resolution of 224×224 pixels. To ensure the same resolution for all images used in model training, despite being collected at different resolutions (digitized at 300 dpi and then cropped to a size of 800 × 600 pixels), they are resized to a final resolution of 224 × 224 pixels prior to model training. Resizing was done using bicubic interpolation method to avoid loss of lesion boundaries andfine detail structure. The preprocessing pipeline was executed in a predefined, fixed order: (i) resampling at a fixed size of 224 × 224, (ii) application of Gaussian filter for noise reduction and lesion morphology preservation, and(iii) normalization of pixel intensity values into the range [0,1]. This standardized preprocessing pipeline maintains uniform input dimension, mitigates noiseinduced variability, and enhances training stability and generalization for all experiments The dataset contains images belonging to seven distinct skin lesion classes. These include Melanocytic nevi (nv) with 6,705 images, which represent the majority class, followed by Melanoma (mel) with 1,113 images, a critical malignant category. Benign keratosis-like lesions (bkl) comprise 1,099 images, while Basal cell carcinoma (bcc) includes 514 images. The dataset also contains Actinic keratoses and intraepithelial carcinoma (akiec) with 327 images, Vascular lesions (vasc) with 142 images, and Dermatofibroma (df) with 115 images, as shown in Figure 2. Due to its class imbalance and clinical relevance, the HAM10000 dataset is extensively used to evaluate and compare advanced machine learning and deep learning models for automated skin cancer detection and classification.

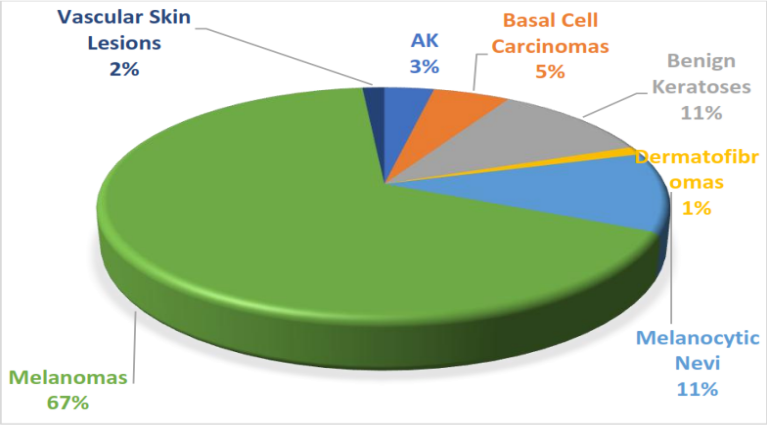

Figure 2: Schematic Representation for the distribution of Skin Lesion Categories in the HAM10000 Dataset

3.2 Pre-Processing

In this research, a structured pre-processing pipeline is proposed to improve the quality of dermoscopic images prior to feature extraction and classification. The pipeline consists of three key steps, namely, resizing, Gaussian filtering, and normalization, ensuring improved model performance and robustness. To maintain uniformity across all images, each dermoscopic image is resized to a fixed dimension (e.g., 224×224 pixels) using bicubic interpolation. This stage ensures uniformity in input dimensions, avoiding complications arising from differing resolutions while preserving critical lesion details [52]. Standardizing image dimensions is essential for deep learning models, as it facilitates effective feature extraction and enhances computing efficiency [53]. A Gaussian filter is utilized to attenuate high-frequency noise while preserving critical lesion features. The Gaussian kernel size is selected empirically according to the dataset features to achieve effective smoothing while minimizing excessive blurring. This phase augments contrast and diminishes extraneous artifacts, hence

enhancing the precision of segmentation and feature extraction [54]. Gaussian filtering is widely used in medical image preprocessing to enhance the appearance of skin diseases while preserving essential morphological characteristics. Shanila et al. [55] contend that medical image analysis requires pre-processing to diminish noise and improve image quality, hence enhancing segmentation efficacy. Furthermore, the Gaussian filter effectively smooths images by reducing high-frequency noise while preserving critical structural information.

To standardize pixel intensity values and optimize convergence during training, min-max normalization is employed, scaling pixel values within the range [0,1] using Equation (1)

$$I' = \frac{I - I_{\min}}{I_{\max} - I_{\min}} \tag{1}$$

where I_{min} and I_{max} denote the minimum and maximum pixel values, respectively. This guarantees a consistent intensity distribution, mitigating bias caused by fluctuating illumination conditions [56]. Effective normalization is crucial in deep learning-driven medical image analysis, since it stabilizes gradients and enhances the learning process [58]. Pre-processing improves the quality of input images, making them better suited for subsequent feature extraction and classification in skin cancer detection models. The proposed strategy enhances model generalization and decreases computational complexity by maintaining uniform picture characteristics.

3.3 Architecture of ResNet50V2.5

In this research, multiple ResNet architectures, namely, ResNet50, ResNet50V2, ResNet50V2.5, ResNet101, and ResNet101V2, for melanoma classification using the HAM10000 dataset have been evaluated. ResNet50 employs a 50-layer deep residual network with bottleneck residual blocks that help reduce computational cost while maintaining performance. ResNet50V2 introduces pre-activation residual blocks, where batch normalization and ReLU activation precede the convolutional layers, leading to better gradient flow and stability during training. ResNet50V2.5 is a fine-tuned intermediate variant that modifies hyperparameters and training strategies of ResNet50V2 to enhance classification performance, particularly on imbalanced medical datasets. ResNet101 extends the architecture to 101 layers, with a deeper stack of residual blocks, allowing it to capture more complex hierarchical features at the cost of increased computational cost. ResNet101V2, similar to ResNet50V2, integrates the pre-activation scheme in its deeper architecture, improving convergence and generalization while addressing vanishing gradient issues in very deep networks.

The ResNet50V2 architecture is a deep CNN variant, enhancing image recognition with improved residual learning and batch normalization techniques. It features a revised residual block structure, pre-activation, and a more efficient network design, achieving state-of-the-art performance across various image classification tasks while reducing computational complexity. ResNet, introduced by He et al. [49] revolutionized deep learning by addressing the vanishing gradient problem in very deep neural networks. Unlike traditional CNN architectures, ResNet employs residual learning via skip connections, allowing gradients to propagate directly during backpropagation. The design of ResNet comprises multiple layers, each of which includes residual blocks. A residual block is a structured arrangement of layers that execute a series of operations on the input in order to generate the output. It also incorporates a shortcut link that appends the input to the output data. Multiple variants of the ResNet architecture exist: ResNet18, ResNet34, ResNet50, ResNet101, and ResNet152. The number in each variation is directly proportional to the number of layers present in the Network. For instance, ResNet50 has 50 layers, whereas ResNet152 has 152 layers. A widely used variation, the ResNet50 architecture is characterized by its five stages, each comprising multiple residual blocks. The initial phase comprises a convolutional layer succeeded by a max-pooling layer, which significantly decreases the spatial dimensions of the input. In the proposed system, we introduce ResNet50V2.5, an enhanced version of the ResNet50V2 architecture, optimized for skin cancer detection. This modification builds upon the strengths of the ResNet family by improving training stability, feature extraction, and classification performance. Figure 3 represents the architecture of the proposed ResNet-based melanoma classification system.

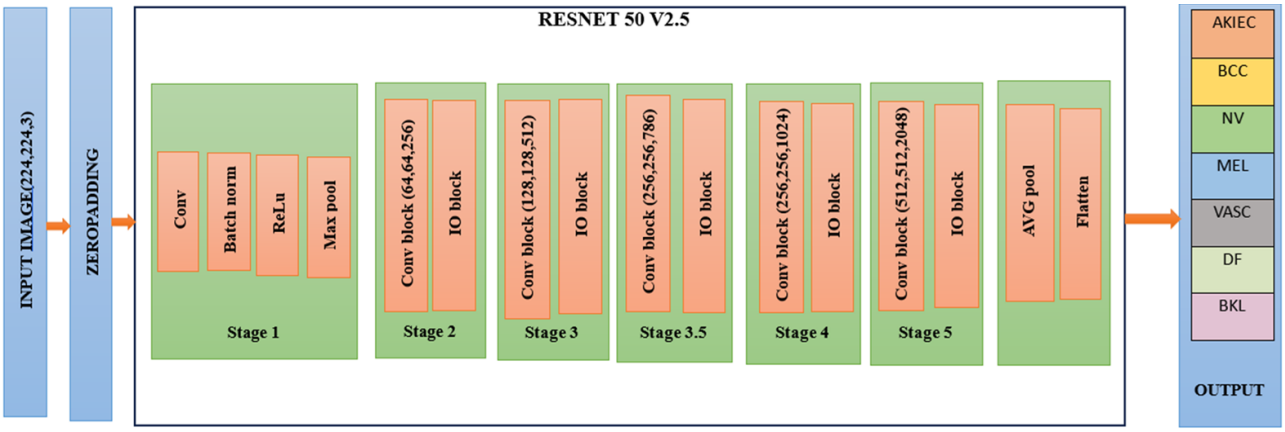

Figure 3: Schematic Representation of the Architecture of the proposed ResNet based Melanoma Classification System

ResNet V2.5 is a sophisticated deep residual network design that enhances ResNetV2 by incorporating pre-activation residual blocks, using batch normalization prior to convolutions, and adding an intermediary stage to improve gradient flow and stability [49]. The design begins with an input image, followed by zero padding and Stage 1, which includes max pooling, batch normalizing, ReLU activation, and convolutional layers [57]. The following stages (2-5) include bottleneck convolutional blocks with varying filter sizes, namely, (64,64,256), (128,128,512), (256,256,786), (256,256,1024), and (512,512,2048), respectively. Stage 3.5, introduced between Stages 3 and 4, enhances feature transfer and reduces information loss, leading to more cohesive learning [58]. The final processing stage includes an input-output (IO) block, global average pooling (AVG Pool), flattening, and a fully connected layer for classification. ResNet V2.5 demonstrates enhanced convergence during training, superior feature extraction, and increased accuracy relative to its predecessors, while maintaining high computational efficiency [59]. Experimental results on benchmark datasets show improved performance compared to ResNetV1 and V2. These adjustments align with advances in deep learning architectures, rendering ResNetV2.5 exceptionally proficient for intricate image identification problems.

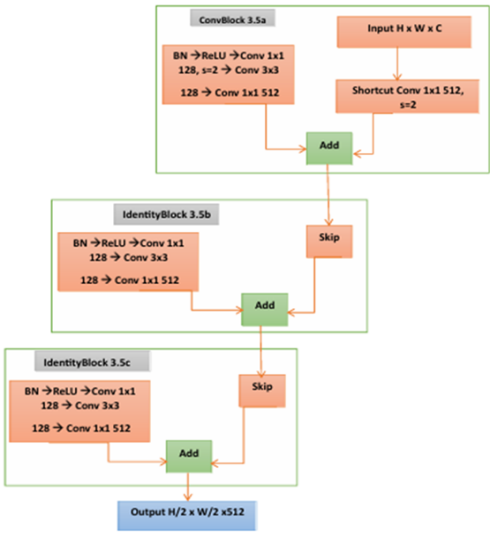

Figure 4: Schematic Representation of a basic Residual block used in the proposed ResNetV2.5 Architecture for Melanoma Classification

Figure 4 depicts a segment of a deep residual network, specifically demonstrating a ResNet block consisting of one convolutional block succeeded by two identity blocks. The architecture initiates with ConvBlock 3.5a,

which receives an input of dimensions H×W×C and executes a sequence of operations: batch normalization, ReLU activation, and three convolutional layers (1×1, 3×3, and 1×1) with channel depths of 128, 128, and 512, respectively. This block features a shortcut link with a 1×1 convolution with 512 filters and a stride of 2 to align the output dimensions with the main path. The outputs of the shortcut and the main pathway are combined element-wise. Subsequently, two identity blocks (3.5b and 3.5c) are arranged in succession, each maintaining the input dimensions.

Hyperparameters	**Value**
Input Image Dimension	256 × 256 pixels
Kernel Size	7×7 & 3 × 3
Max Pooling	3 × 3
Padding	Valid & Same
Activation Functions	ReLU & SoftMax
Optimizer	Adam
Loss Function	sparse_categorical_crossentropy
Batch Size	32
Learning Rate	Varied: 1e-5
Epochs	20

Table 1: Hyperparameters used in the proposed ResNet 50 V2.5 based skin cancer Classification

Algorithm 1: Classification of ResNet50V2.5 Archiecture

INPUT: input_shape = (256,256,3), num_classes = 7
OUTPUT: model
X ← Input(input_shape)
Initial stem
X ← ZeroPad(3) → Conv7×7,64,s2 → BN → ReLU → MaxPool3×3,s2
Residual stages (Pre-activation bottleneck blocks)
Each stage: [filters], first block = ConvBlock, rest = IdentityBlocks
Stage 2: [64,64,256], stride=1
X ← ConvBlock(X)
X ← IdentityBlock × 2
Stage 3: [128,128,512], stride=2
X ← ConvBlock(X)
X ← IdentityBlock × 3
Stage 3.5 (Proposed): [192,192,768], stride=2
X ← ConvBlock(X)
X ← IdentityBlock × 4
Stage 4[256,256,1024], stride=2
X ← ConvBlock(X)
X ← IdentityBlock × 5
Stage 5: [512,512,2048], stride=2
X ← ConvBlock(X)
X ← IdentityBlock × 6
Classification head
X ← AvgPool → Flatten → Dense(num_classes, Softmax)
RETURN Model(Input, X)
END

These blocks perform similar convolutional operations, such as 1×1 → 3×3 → 1×1 convolutions with 128, 128, and 512 filters, respectively, but also include direct skip connections, meaning the input is passed forward without transformation. In each identity block, the input is added to the processed output to form the final feature map. The overall output of this sequence is a feature map of reduced spatial size H/2×W/2, with an increased depth of 512 channels, enabling deeper representation learning with minimized vanishing gradient issues. The Hyperparameters used in the proposed Resnet 50 V2.5 based skin cancer classification is given in Table 1 and Algorithm 1 represents the Classification of the proposed ResNet based Melanoma Classification System

3.4 Performance Metrics Used

Performance metrics for skin cancer detection often encompass accuracy [60], precision, recall, F1 score, Matthews Correlation Coefficient, Cohens Kappa, Hamming Loss, Jaccard Score and area under the receiver operating characteristic curve (AUC-ROC), which evaluate the efficacy of classification algorithms. These metrics assess the model's efficacy in identifying malignant lesions, reducing false positives and false negatives, and generalizing to novel data, hence assuring robust and reliable performance in clinical environments.

- **Accuracy:** Accuracy measures the ratio of correct predictions to the total predictions made by the model. It provides a basic performance metric, calculated using Equation (2).

$$Accuracy = \frac{TP + TN}{TP + TN + FP + FN} \tag{2}$$

- **Precision and Recall:** The need for precision in minimizing false positives is crucial in clinical settings to prevent the categorization of benign cases as malignant. Concurrently, recall (or sensitivity) is highlighted as essential for the accurate identification of malignant cases, computed using Equations (3) and (4) respectively.

$$Precision = \frac{TP}{TP + FP} \tag{3}$$

$$Recall = \frac{TP}{TP + FN} \tag{4}$$

- **F1-Score:** This metric is highlighted for its fair methodology, especially with imbalanced datasets, ensuring the maintenance of both high precision and recall. The F1-Score is calculated using Equation (5).

$$F1 - Score = 2 \times \frac{Precision \times Recall}{Precision + Recall} \tag{5}$$

- **Matthews Correlation Coefficient (MCC):** MCC is a balanced measure that takes into account true positives, true negatives, false positives, and false negatives, providing a single value metric that works well even with imbalanced datasets, which is calculated using Equation (6).

$$MCC = \frac{TP \times TN - FP \times FN}{\sqrt{(TP + FP)(TP + FN)(TN + FP)(TN + FN)}} \tag{6}$$

  where True Positive (TP) represents the correctly predicted positive cases, False Positive (FP) refers to incorrectly predicted as positive (type I error), False Negative (FN) means incorrectly predicted as negative (type II error), and True Negative (TN) means correctly predicted negative cases.

- **Cohen's Kappa:** Cohen's Kappa measures inter-rater agreement, accounting for agreement occurring by chance. The Cohen's Kappa is calculated using Equation (7).

$$k = \frac{P_0 - P_e}{1 - P_e} \tag{7}$$

where, P_0 is the observed agreement. P_e is the expected agreement by chance (calculated based on the marginal probabilities of each rater).

- **Hamming Loss:** Hamming Loss quantifies misclassification in multi-label classification tasks by identifying incorrect label predictions. Hamming Loss varies from 0 (indicating flawless classification with no erroneous labels) to 1 (signifying complete misclassification of all labels). The Hamming Loss is calculated using Equation (8).

$$Hamming\ Loss = \frac{1}{N * L} \sum_{i=1}^{N} \sum_{j=1}^{L} I\left(y_{ij} \neq \widehat{y_{ij}}\right) \tag{8}$$

where, N = Total number of instances (samples), L = Total number of labels, y_{ij} = True label (0 or 1) for instance i and label *j*, and $\widehat{y_t}$ = Predicted label (0 or 1) for instance *i* and label *j*

- **Jaccard Score:** The Jaccard Index (also known as the Jaccard Similarity Coefficient) is a metric used to measure the similarity between two sets. The Jaccard Index is used to evaluate how well the predicted segmentation (e.g., tumour boundaries) matches the ground truth (manual or expert annotations). The Jaccard Index is calculated using Equation (9).

$$Jaccard\ Index = \frac{|A \cap B|}{|A \cup B|} \tag{9}$$

where, A = Set of elements in the first set (e.g., predicted labels or pixels in segmentation), B = Set of elements in the second set (e.g., true labels or pixels in ground truth segmentation), $|A \cap B|$ = Number of common elements (True Positives) and $|A \cup B|$ = Total number of elements in both sets (True Positives + False Positives)

4 Experimental Results and Discussion

The HAM10000 (Human Against Machine) dataset, comprising 10,015 Dermatoscopic images, was employed for skin lesion classification. The experimental setup involved implementing a ResNet model. The dataset was split into training and test sets at 80:20, and cross-validation was used to improve model performance. The entire operation was executed using Python 3.10 within Visual Studio Code. The system configuration included an Intel 10th Generation i5 processor, 16GB of RAM, and an Nvidia GeForce RTX 3060 GPU with 12GB of memory, running either Windows 10 or Ubuntu 20.04. This paper evaluates the effectiveness of various ResNet architectures in melanoma classification, namely ResNet101, ResNet101V2, ResNet50, ResNet50V2, and ResNet50V2.5, employing a publicly available melanoma dataset. ResNet50V2.5 exhibited enhanced classification performance relative to other architectures, achieving an accuracy of 99.17%, as demonstrated in Table 1. The model reliably differentiated between melanoma and non-melanoma cases, as evidenced by critical evaluation metrics. A precision of 99.24% indicated a negligible false-positive rate, while a recall of 99.20% exhibited strong sensitivity in detecting melanoma patients. The model's exceptional classification ability was confirmed by its F1-score (99.19%), Matthews Correlation Coefficient (98.88%), and Cohen's Kappa (98.87%), all indicating a strong agreement between predicted and actual labels. Moreover, it demonstrated the lowest Hamming Loss (0.80%) and the highest Jaccard Score (97.47%), indicating minimal misclassification and strong predictive efficacy.

The training and validation accuracy curves exhibited a consistent improvement in learning throughout 25 epochs, resulting in a final accuracy of 92%, indicating effective generalization to the validation dataset. The training and validation loss curves showed a steady decline, and later epochs indicated convergence with minimal overfitting. The results demonstrated that the ResNet50V2.5 model is an effective tool for melanoma classification, offering a balance of high accuracy, sensitivity, and specificity. Its strong performance across

various evaluation metrics makes it a valuable instrument for assisting medical professionals in the early and accurate detection of melanoma, hence improving patient outcomes.

ResNet101V2 exceeded both ResNet50 and ResNet101, with an accuracy of 94.9%. This model exhibited a precision of 95.4%, a recall of 94.9%, and an F1-score of 95%, demonstrating a strong balance between sensitivity and specificity. Its MCC (94.1%), Cohen's Kappa (94.1%), and Jaccard Score (90.7%) further corroborated its outstanding reliability in melanoma classification. Moreover, its diminished Hamming Loss (5.04%) compared to ResNet101 indicates fewer classification errors, making it a more dependable model. Table 2 presents the performance metrics for all ResNet models on the HAM10000 dataset.

Models	Precision (%)	F1-Score (%)	Jaccard Score (%)	Recall (%)	MCC (%)	Hamming Loss (%)	Kappa (%)	Accuracy (%)
ResNet 50	87.90	86.80	81.30	86.70	84.80	10.10	84.60	90%
ResNet 101	92.3	91 .9	85.7	91.9	90.5	8.10	90.50	91.80
ResNet 101V2	95.4	95.0	90.7	94.9	94.10	5.04	94.10	94.90
ResNet 50 V2	97.50	98.40	97.60	97.20	97.60	2.80	97.50	98.20
ResNet 50 V2.5	99.24	99.19	97.47	99.20	98.88	0.80	98.87	99.17
ResNet 50 V2.5 (ISIC 2019)	97.83	97.72	96.34	97.70	97.34	2.3	87.33	97.71

Table 2: Performance Comparison of Quantifying Parameters of the proposed ResNet models for Skin Cancer Classification using the HAM10000 dataset

ResNet50 achieved 90% accuracy, making it a competitive model; however, it fell short compared to ResNet 101 and more advanced versions. The model achieved classification accuracy of 87.9%, precision of 87.9%, recall of 86.7%, and an F1-score of 86.8%. However, its Jaccard Score (81.3%) and MCC (84.8%) indicate that it was slightly less effective in distinguishing between melanoma and non-melanoma individuals. The model has a Hamming Loss of 10.1%, indicating a higher misclassification rate than ResNet101 and more recent architectures.

ResNet50V2 demonstrated superior performance, with an accuracy of 98.2%. This model achieved a remarkable precision of 97.5%, a recall of 97.2%, and an F1-score of 98.4%, demonstrating robust classification performance. The MCC (97.6%) and Cohen's Kappa (97.5%) demonstrated a strong association with the actual labels. The Jaccard Score of 97.6% and a notably low Hamming Loss of 1.8% show enhanced generalization and robustness relative to previous models.

The accuracy progression of five ResNet architectures, namely, ResNet50, ResNet101, ResNet101V2, ResNet 50V2, and ResNet50V2.5, across epochs 15, 20, and 25 (Figure 5) shows continual performance gains, highlighting their learning and generalization ability. ResNet50 and ResNet101 improve from 77.20% and 75.40% at epoch 15 to 90% and 91.80% at epoch 25. In contrast, ResNet50V2 and ResNet50V2.5 achieve much higher results, improving from 95.30% and 97.20% to 98.20% and 99.17% over the same epochs, with ResNet50V2.5 performing best. Figure 5 further shows that ResNet50 and ResNet101 maintain stable accuracy with minimal divergence between training and validation, whereas ResNet101V2 exhibits fluctuations in validation accuracy, suggesting potential overfitting. ResNet50V2 and ResNet50V2.5 converge more smoothly, with validation curves closely following training curves, confirming robust generalization and stability. Figure 6 shows the model loss curves across training epochs. ResNet50 reduces both losses smoothly with minor fluctuations, while ResNet101 shows an even steadier validation curve, indicating stronger generalization. ResNet101V2 decreases training loss rapidly but has unstable validation loss with sharp spikes, revealing overfitting. ResNet50V2 maintains smoother training with moderate fluctuations in validation loss, suggesting mild overfitting. ResNet50V2.5 achieves the most balanced performance, with training and validation losses consistently close and converging near zero, reflecting excellent generalization. Overall, ResNet50V2.5 performs best, followed by ResNet101 and ResNet50, while ResNet101V2 shows instability. Figure 6 illustrates the confusion matrices. ResNet50 provides a solid baseline with some neighbouring misclassifications.

ResNet101 improves diagonal dominance and reduces errors, though some remain in classes such as 0 and 6. ResNet101V2 improves stability with fewer misclassifications, while ResNet50V2 further enhances diagonal alignment. ResNet50V2.5 produces the cleanest matrix with minimal off-diagonal errors, confirming superior accuracy and robustness. The ROC curves depicted in Figure 8 for ResNet101V2, ResNet50, ResNet50V2, and ResNet50V2.5 demonstrate exceptional classification performance where Class 0 corresponds to melanoma, Class 1 to melanocytic nevus, Class 2 to basal cell carcinoma, Class 3 to actinic keratosis, Class 4 to benign keratosis, Class 5 to dermatofibroma, and Class 6 to vascular lesion, reflecting the seven categories defined in the HAM10000 dataset.

ResNet101V2 exhibits strong discriminatory ability, with AUC values ranging from 0.93 to 1.00. Classes 2, 3, 4, and 5 exhibit near-perfect separability (AUC ¿ 0.99), whereas classes 0, 1, and 6 yield slightly lower but still elevated AUC values (0.930.97). ResNet50 achieves a consistently high AUC across all classes, ensuring perfect discrimination, while ResNet101 demonstrates commendable performance, with most classes attaining high accuracy and a few slightly lower at 0.99. Similarly, ResNet50V2 and ResNet50V2.5 achieve high AUCs across all classes, indicating impeccable classification performance with no false positives or negatives. The results confirm the models' remarkable ability to distinguish between classes, with ResNet50, ResNet50V2, and ResNet50V2.5 demonstrating absolute accuracy, while ResNet101V2 attains near-perfect classification.

The performance analysis reveals that while ResNet50 and ResNet101 are proficient, the latest versions, ResNet101V2, ResNet 50V2, and ResNet50V2.5, exhibit significant improvements in accuracy, precision, and classification reliability. ResNet50V2.5 emerged as the most efficacious model among those evaluated, establishing it as a significant tool for melanoma detection in clinical environments. The proposed work utilizing ResNet50V2.5 surpasses the current architectures, attaining 99.17% accuracy, 99.24% precision, 99.20% recall, and 99.19% F1-score, exceeding the metrics of Hasan et al. [61], Yin et al. [62], Qin et al. [63], and Javed et al. [64], thereby demonstrating superior performance as shown in Table 3. Also the details regarding the total number of trainable and non-trainable parameters in the proposed RESNET architectures for skin cancer classification is given in Table 4.

Authors	**Architectures**	**Data Set**	**Training: Testing**	**Accuracy (%)**	**Precision (%)**	**Recall (%)**	**F1-score (%)**
Hasan et al. [61]	CNN	ISIC Archive	—-	93.70	83.25	84	83.25
Yin et al. [62]	DenseNet-169	ISIC 2019	75:25	95.41	88.80	89	90
Qin et al. [63]	Style-based GAN	ISIC 2018	——	95.22	96.60	—	—
Javed et al. [64]	MobileNetV2	ISIC 2020	70:30	98.10	98.10	98.3	98.11
ResNet50V2.5 (Proposed Work)	Custom CNN	HAM10000	80:20	99.17	99.24	99.20	99.19

Table 3: Performance Comparison of ResNet50V2.5 with the State-of-the-Art methods for the proposed Melanoma Diagnosis using the HAM10000 dataset

Architectures	**Average Processing Time (20 epoch)**	**Trainable Parameters**	**Non Trainable Parameters**	**Total Parameters**
ResNet 50	1.8 hrs	25,557,032	53,120	25,610,152
ResNet 101	3.2 hrs	44,549,160	53,120	44,602,280
ResNet 101V2	3.4 hrs	44,543,848	55,296	44,599,144
ResNet 50V2	2 hrs	28,225,671	55,296	28,280,967
ResNet 50V2.5	3 hrs	45,275,399	86,784	45,362,183

Table 4: Total number of parameters in the proposed RESNET Architectures for Skin Cancer Classification

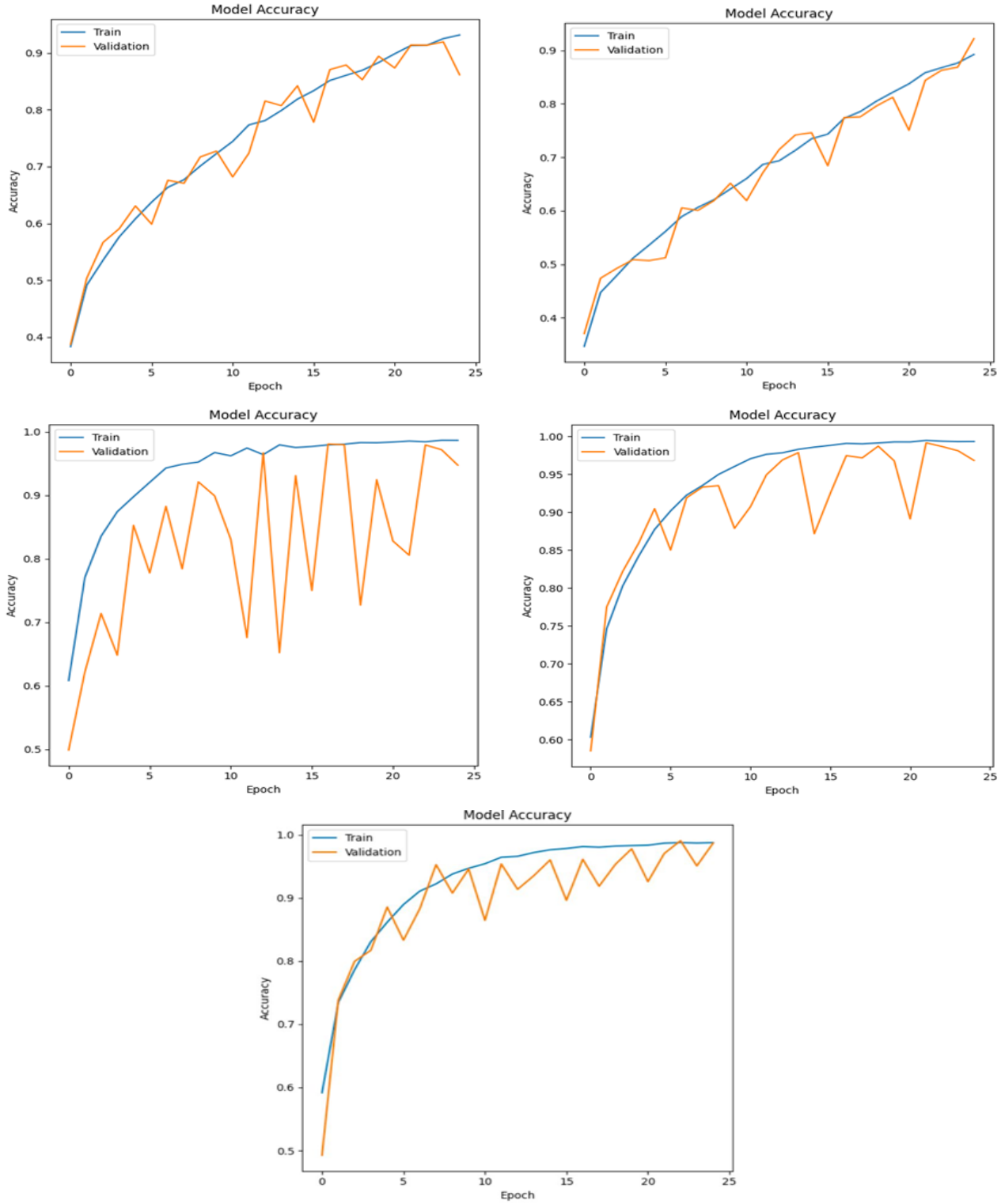

Figure 5: Performance Comparison of Accuracy Curves across ResNet Architectures (From top to Bottom): ResNet 50; ResNet 101; ResNet 101V2; ResNet50V2 and ResNet 50V2.5

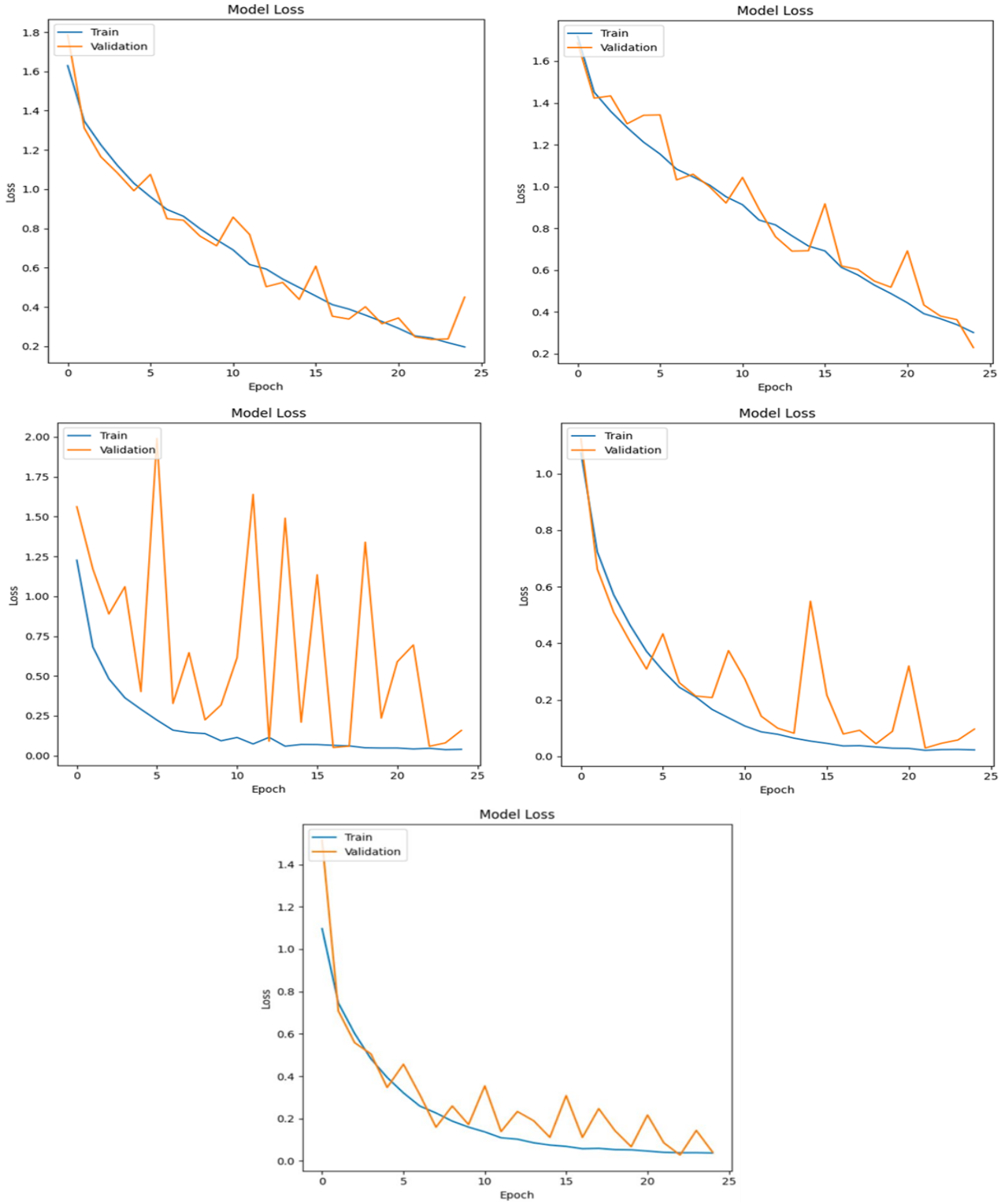

Figure 6: Performance Comparison of Loss Curves across ResNet Architectures (From top to Bottom): ResNet 50; ResNet 101; ResNet 101V2; ResNet50V2 and ResNet 50V2.5

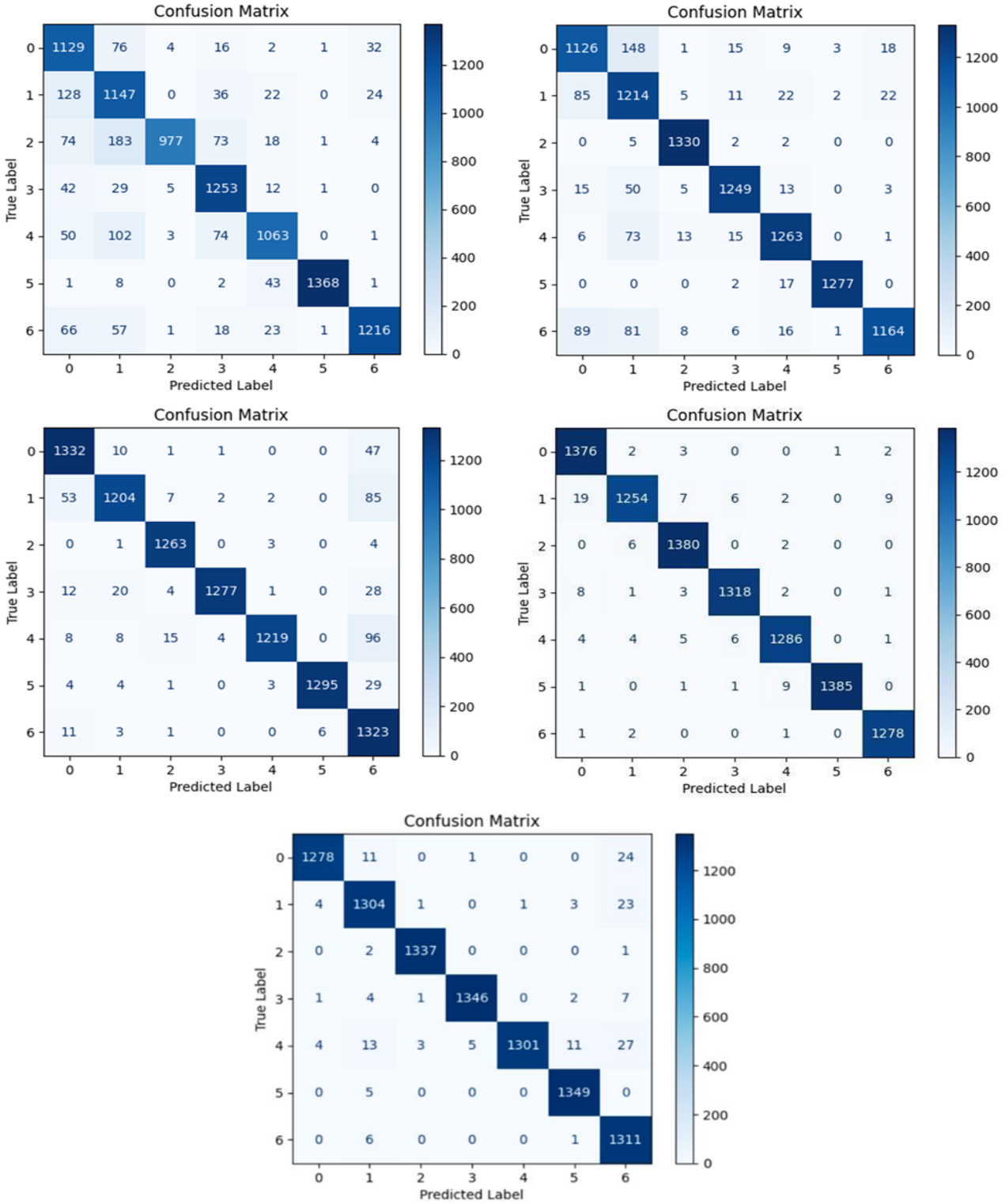

Figure 7: Performance Comparison of Confusion Matrix across ResNet Architectures (From top to Bottom): ResNet 50; ResNet 101; ResNet 101V2; ResNet50V2 and ResNet 50V2.5

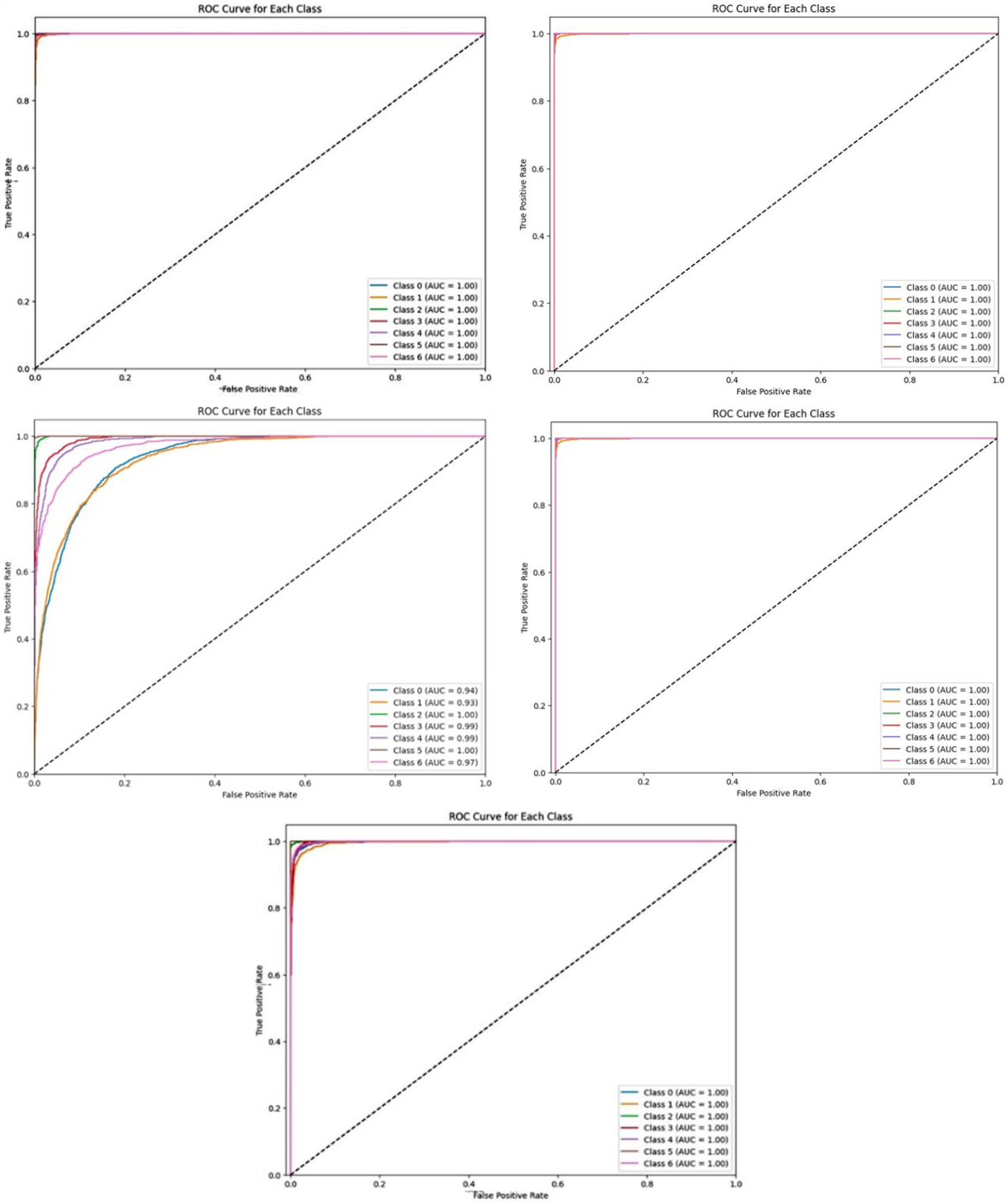

Figure 8: Performance Comparison of ROC Curves (From top to Bottom): ResNet 50; ResNet 101; ResNet 101V2; ResNet50V2 and ResNet 50V2.5.

The experiment was conducted using the ISIC2019 dataset in ResNet50V2.5 model, maintaining identical training, testing, and validation ratios. A total of 80% images were allocated for training, and 10% images each for testing and validation. All relevant quantitative performance metrics were evaluated. The model achieved an

accuracy of 97.71%, approximately 2% lower than that obtained with the HAM10000 dataset, indicating slight performance variation across datasets. Also the performance of other parameters namely precision, recall, F1-score, Jaccard score , Kappa, MCC using ISIC 2019 is less than that of HAM10000 dataset. To address the implications of the high reported accuracy, strict pre-split augmentation was applied to prevent duplicate or overlapping images across subsets, while regularization and early stopping were used to reduce overfitting. Model robustness was further validated through external testing, ensuring the absence of data leakage.

Despite achieving high performance, the custom ResNet50V2 with an added Stage 3.5 may suffer from overfitting due to increased architectural complexity. The models generalization to external datasets and diverse skin tones is unverified. Higher computational cost, limited interpretability, potential class imbalance bias, and lack of clinical metadata integration remain key limitations for real-world deployment.

5 Conclusion

This study describes the deep learning methodologies to categorize skin cancer images into seven distinct classes from the HAM10000 database, following preprocessing through normalization and augmentation to enhance model robustness. A comparison of ResNet variants, namely, ResNet101, ResNet101V2, ResNet50, ResNet50V2, and the newly proposed ResNet50V2.5, demonstrated that ResNet50V2.5 achieved the highest performance, attaining an accuracy of 99.17% on HAM10000. Unlike the conventional ResNet50V2, the proposed architecture introduces a second intermediate residual stage to improve gradient flow, refined bottleneck configurations, and carefully optimized hyperparameters and training protocols. These dual architectural modifications enhance feature representation and training stability, thereby improving the handling of the datasets inherent imbalance. To further examine generalizability, the model was also evaluated on the ISIC2019 dataset, where performance was approximately 2% lower than on HAM10000. While still highly promising, these results highlight the importance of validating on diverse, clinically realistic datasets to mitigate the risk of overfitting.

Despite its strong performance, integrating such AI-driven systems into clinical practice remains challenging. Barriers such as interpretability, clinician trust, regulatory compliance, and interoperability with existing health IT systems must be addressed before real-world deployment. Integrating a ViT with ResNet50V2.5 enables patch-based lesion feature encoding and multi-head self-attention, improving global context modeling, classification accuracy, and generating interpretable attention maps for explainable, robust melanoma diagnosis. Future work will therefore focus on enhancing the framework through hybrid approaches, such as integrating Swin Transformer architectures for superior hierarchical feature extraction, incorporating explainable AI methodologies for transparency, and leveraging multimodal clinical data fusion to improve diagnostic reliability. Future work will also involve testing on real-world, unseen clinical images acquired from diverse devices and patient groups to confirm practical diagnostic robustness beyond curated datasets. Collectively, these advancements may enhance the practical applicability of ResNet50V2.5 as a diagnostic aid, supporting dermatologists in the early and accurate detection of melanoma.

References

[1] S. Khattar and R. Kaur, "Computer assisted diagnosis of skin cancer: A survey and future recommendations", *Computers & Electrical Engineering* 104(1): 108431, 2022. doi: 10.1016/j.compeleceng.2022.108431.

[2] S. Labani, S. Asthana, K. Rathore, and K. Sardana, "Incidence of melanoma and nonmelanoma skin cancers in Indian and the global regions", *Journal of Cancer Research and Therapeutics* 17(4): 906–911, 2020, doi: 10.4103/jcrt.jcrt_785_19.

[3] K. M. Hosny, M. A. Kassem, and M. M. Fouad, "Classification of Skin Lesions into Seven Classes Using Transfer Learning with AlexNet", *Journal of Digital Imaging* 33(5): 1325-1334, 2020, doi: 10.1007/s10278-020-00371-9.

[4] M. A. A. Milton, "Automated skin lesion classification using ensemble of deep neural networks in ISIC 2018: Skin Lesion Analysis towards Melanoma Detection Challenge", *arXiv (Cornell University)* 225–228 2019, doi: 10.48550/arxiv.1901.10802.

[5] M. Q. Khan et al., "Classification of melanoma and nevus in digital images for diagnosis of skin cancer", *IEEE Access* 7(1): 90132-90144, 2019, doi: 10.1109/access. 2019.2926837.

[6] H. Tsao et al., "Early detection of melanoma: Reviewing the ABCDEs", *Journal of the American Academy of Dermatology* 72(4): 717-723, 2015, doi: 10.1016/j. jaad.2015.01.025.

[7] H. Alquran et al., "The melanoma skin cancer detection and classification using support vector machine", *In 2017 IEEE Jordan Conference on Applied Electrical Engineering and Computing Technologies (AEECT)*, pp. 1-5, 2017, doi: 10.1109/aeect.2017.8257738.

[8] M. Strzelecki, M. Kocioek, M. Strkowska, M. Kozowski, A. Grzybowski, and P. M. Szczypiski, "Artificial intelligence in the detection of skin cancer: State of the art", *Clinics in Dermatology* 42(3): 280-295, 2024, doi: 10.1016/j.clindermatol. 2023.12.022.

[9] E. J. Beltrami, A. C. Brown, P. J. M. Salmon, D. J. Leffell, J. M. Ko, and J. M. Grant-Kels, "Artificial intelligence in the detection of skin cancer", *Journal of the American Academy of Dermatology*, 87(6): 1336-1342, 2022, doi: 10.1016/j.jaad.2022.08.028.

[10] U. Leiter, U. Keim, and C. Garbe, "Epidemiology of Skin Cancer: Update 2019", *Advances in Experimental Medicine and Biology* 1268(1): 123-139, 2020, doi: 10.1007/978-3-030-46227-7_6.

[11] M. M. Taye, "Understanding of Machine Learning with Deep Learning: Architectures, Workflow, Applications and Future Directions", *Journal of Computers*, 12(5): 91–99, 2023, doi: 10.3390/computers12050091.

[12] D. Valkenborg, M. Geubbelmans, A.-J. Rousseau, and T. Burzykowski, "Supervised learning", *American Journal of Orthodontics and Dentofacial Orthopedics*, 164(1): 146-149, 2023, doi: 10.1016/j.ajodo.2023.04.010.

[13] J. M. Duarte and L. Berton, "A review of semi-supervised learning for text classification", *Artificial Intelligence Review* 56(9): 9401-9469, 2023, doi: 10.1007/s10462-023-10393-8.

[14] D. Valkenborg, A.-J. Rousseau, M. Geubbelmans, and T. Burzykowski, "Unsupervised learning", *American Journal of Orthodontics and Dentofacial Orthopedics* 163(6): 877-882, 2023, doi: 10.1016/j.ajodo.2023.04.001.

[15] A. Adegun and S. Viriri, "Deep learning techniques for skin lesion analysis and melanoma cancer detection: a survey of state-of-the-art", *Artificial Intelligence Review* 54(2): 811-841, 2020, doi: 10.1007/s10462-020-09865-y.

[16] M. Lee, "Deep Learning Techniques with Genomic Data in Cancer Prognosis: A Comprehensive Review of the 20212023 Literature", *Biology*, 12(7): 893–900, 2023. doi: 10.3390/biology12070893.

[17] Chen, C. L., Srinivasulu, A., Ravikumar, C. V., Ganesh, G. V., Sreenivasulu, G., Karuna, Y., & Deng, Y. Y., Estimation of Skin Cancer with Integrated Extended Convolutional and Recurrent Neural Network Techniques on Image Dataset, *Journal of Research in Engineering and Computer Sciences*, 1(3): 15–32, 2023.

[18] Koo. KC, Lee. KS, Kim. S, Min. C, Min. GR, Lee. YH, Han. WK, Rha. KH, Hong. SJ, Yang. SC, Chung. BH, "Long short-term memory artificial neural network model for prediction of prostate cancer survival outcomes according to initial treatment strategy: development of an online decision-making support system", *World Journal of Urology* 38(10): 2469-2476, 2020. doi: 10.1007/s00345-020-03080-8.

[19] A. H. Shahin, A. Kamal, and M. A. Elattar, "Deep Ensemble Learning for Skin Lesion Classification from Dermoscopic Images", *In 2018, 9th Cairo International Biomedical Engineering Conference (CIBEC)*, pp. 150-153, 2018. doi: 10.1109/cibec.2018. 8641815.

[20] A. Masood and A. A. Al-Jumaily, "Computer Aided Diagnostic Support System for Skin Cancer: A review of Techniques and Algorithms", *International Journal of Biomedical Imaging*, 2013(1): 1-22, 2013. doi: 10.1155/2013/323268.

[21] H. Kittler, H. Pehamberger, K. Wolff, and M. Binder, "Diagnostic accuracy of dermoscopy", *The Lancet Oncology* 3(3): 159-165, 2002. doi: 10.1016/s1470-2045(02)00679-4.

[22] B. Erkol, R. H. Moss, R. J. Stanley, W. V. Stoecker, and E. Hvatum, "Automatic lesion boundary detection in dermoscopy images using gradient vector flow snakes", *Skin Research and Technology* 11(1): 17-26, 2005. doi: 10.1111/j.1600-0846.2005.00092.x.

[23] M. Zorman, M. M. tiglic, P. Kokol, and I. Mali, "The limitations of decision trees and automatic learning in real world medical decision making", *Journal of Medical Systems* 21(6): 403-415, 1997. doi: 10.1023/a:1022876330390.

[24] W. Loh, "Classification and regression trees", *Wiley Interdisciplinary Reviews Data Mining and Knowledge Discovery* 1(1): 14-23, 2011. doi:10.1002/widm.8.

[25] K. Larsen, "Generalized naive Bayes classifiers", *ACM SIGKDD Explorations Newsletter*, 7(1), 7681, 2005. doi: 10.1145/1089815.1089826.

[26] D. Ruiz, V. Berenguer, A. Soriano, and B. Sanchez, "A decision support system for the diagnosis of melanoma: A comparative approach", *Expert Systems With Applications* 38(12): 1521715223, 2011. doi: 10.1016/j.eswa.2011.05.079.

[27] S. Gilmore, R. HofmannWellenhof, and H. P. Soyer, "A support vector machine for decision support in melanoma recognition", *Experimental Dermatology*, 19(9): 830-835, 2010. doi: 10.1111/j.1600-0625.2010.01112.x.

[28] D. Silver et al., "Mastering the game of Go with deep neural networks and tree search", *Nature* 529(7587): 484-489, 2016, doi: 10.1038/nature16961.

[29] N. Codella, J. Cai, M. Abedini, R. Garnavi, A. Halpern, and J. R. Smith, "Deep learning, sparse coding, and SVM for melanoma recognition in dermoscopy images", *in Lecture notes in computer science*, pp. 118-126, 2015. doi: 10.1007/978-3-319-24888-2_15.

[30] K. Fukushima, "Neocognitron: A hierarchical neural network capable of visual pattern recognition", *Neural Networks* 1(2): 119-130, 1988, doi: 10.1016/0893-6080(88)90014-7.

[31] LeCun, Y., Kanter, I., & Solla, S., Second order properties of error surfaces: Learning time and generalization, *Advances in neural information processing systems*, 3(1): 841–850, 1990.

[32] A. Esteva et al., "Dermatologist-level classification of skin cancer with deep neural networks", *Nature* 542(7639), 115118, 2017, doi: 10.1038/nature21056.

[33] L. Yu, H. Chen, Q. Dou, J. Qin, and P.-A. Heng, "Automated melanoma recognition in dermoscopy images via very deep residual networks", *IEEE Transactions on Medical Imaging* 36(4): 9941004, 2016, doi: 10.1109/tmi.2016.2642839.

[34] U.-O. Dorj, K.-K. Lee, J.-Y. Choi, and M. Lee, "The skin cancer classification using deep convolutional neural network", *Multimedia Tools and Applications* 77(8) 99099924, 2018. doi: 10.1007/s11042-018-5714-1.

[35] S. S. Han, M. S. Kim, W. Lim, G. H. Park, I. Park, and S. E. Chang, "Classification of the clinical images for benign and malignant cutaneous tumors using a deep learning algorithm", *Journal of Investigative Dermatology* 138(7): 15291538, 2018. doi: 10.1016/j.jid.2018.01.028.

[36] D. Roffman, G. Hart, M. Girardi, C. J. Ko, and J. Deng, "Predicting non-melanoma skin cancer via a multi-parameterized artificial neural network", *Scientific Reports* 8(1): 1701–1711, 2018. doi: 10.1038/s41598-018-19907-9.

[37] A. Murugan, S. A. H. Nair, A. A. P. Preethi, and K. P. S. Kumar, "Diagnosis of skin cancer using machine learning techniques", *Microprocessors and Microsystems* 81(1): 103727–103735, 2020. doi: 10.1016/j.micpro.2020.103727.

[38] J. V. Tembhurne, N. Hebbar, H. Y. Patil, and T. Diwan, "Skin cancer detection using ensemble of machine learning and deep learning techniques", *Multimedia Tools and Applications* 82(18): 27501-27524, 2023. doi: 10.1007/s11042-023-14697-3.

[39] M. Vidya and M. V. Karki, "Skin Cancer Detection using Machine Learning Techniques", *In 2020 IEEE International Conference on Electronics, Computing and Communication Technologies (CONECCT)*, pp. 15, Jul. 2020. doi: 10.1109/ conecct50063.2020.9198489.

[40] P. P. Tumpa and M. A. Kabir, "An artificial neural network based detection and classification of melanoma skin cancer using hybrid texture features", *Sensors International* 2(1): 100128–100136, 2021. doi: 10.1016/j.sintl.2021.100128.

[41] S. Sugiarti, Y. Yuhandri, J. Naam, D. Indra, and J. Santony, "An artificial neural network approach for detecting skin cancer", *TELKOMNIKA (Telecommunication Computing Electronics and Control)* 17(2): 788–796, 2019. doi: 10.12928/ telkomnika.v17i2.9547.

[42] M. Kumar, M. Alshehri, R. AlGhamdi, P. Sharma, and V. Deep, "A DE-ANN inspired skin cancer detection approach using fuzzy C-Means clustering", *Mobile Networks and Applications* 25(4): 13191329, 2020, doi: 10.1007/s11036-020-01550-2.

[43] M. Nawaz et al., "Skin cancer detection from dermoscopic images using deep learning and fuzzy kmeans clustering", *Microscopy Research and Technique* 85(1): 339351, 2021, doi: 10.1002/jemt.23908.

[44] R. R. Subramanian, D. Achuth, P. S. Kumar, K. N. K. Reddy, S. Amara, and A. S. Chowdary, "Skin cancer classification using Convolutional neural networks", *In 2021 11th International Conference on Cloud Computing, Data Science & Engineering (Confluence)* pp. 1319, 2021. doi: 10.1109/confluence51648.2021.9377155.

[45] N. Rezaoana, M. S. Hossain, and K. Andersson, "Detection and classification of skin cancer by using a parallel CNN model", *2020 IEEE International Women in Engineering (WIE) Conference on Electrical and Computer Engineering (WIECON-ECE)*, pp. 380386, 2020. doi: 10.1109/wiecon-ece52138.2020.9397987.

[46] N. Gouda and J. Amudha, "Skin Cancer Classification using ResNet", *In 2020 IEEE 5th International Conference on Computing Communication and Automation (ICCCA)*, pp. 536541, 2020, doi: 10.1109/iccca49541.2020.9250855.

[47] A. Budhiman, S. Suyanto, and A. Arifianto, "Melanoma Cancer Classification Using ResNet with Data Augmentation", *2019 International Seminar on Research of Information Technology and Intelligent Systems (ISRITI)*, pp. 1720, 2019. doi: 10.1109/ isriti 48646.2019.9034624.

[48] A. Mehra, A. Bhati, A. Kumar, and R. Malhotra, "Skin cancer classification through transfer learning using REsNEt-50", *in Advances in intelligent systems and computing*, pp. 5562, 2021. doi: 10.1007/978-981-33-4367-2_6.

[49] K. He, X. Zhang, S. Ren, and J. Sun, "Deep Residual Learning for Image Recognition", *In Proceedings of the IEEE Conference on Computer Vision and Pattern Recognition*, pp. 770778, 2016. doi: 10.1109/cvpr.2016.90.

[50] P. Tschandl, C. Rosendahl, and H. Kittler, "The HAM10000 dataset, a large collection of multi-source dermatoscopic images of common pigmented skin lesions", *Scientific Data* 5(1): 180161–180170, 2018. doi: 10.1038/sdata.2018.161.

[51] Lameski, P., Simjanoska, M., & Dimitrov, S, Preprocessing techniques for medical image analysis: A case study on skin lesion detection, *International Journal of Computer Vision and Image Processing* 8(1): 35–49, 2018.

[52] Codella, N. C. F., Gutman, D., Celebi, M. E., Helba, B., & Halpern, A. (2018). Skin lesion analysis toward melanoma detection, *IEEE Journal of Biomedical and Health Informatics* 23(2): 501–510, 2016. DOI:10.48550/arXiv.1710.05006

[53] M. E. Celebi et al., "A methodological approach to the classification of dermoscopy images", *Computerized Medical Imaging and Graphics*, 31(6): 362-373, 2007. doi: 10.1016/j.compmedimag.2007.01.003.

[54] J. Kawahara, A. BenTaieb, and G. Hamarneh, "Deep features to classify skin lesions", *IEEE Transactions on Biomedical Engineering* 21(6): 13971400, 2016. doi: 10.1109/ isbi.2016.7493528.

[55] N. Shanila, R. S. V. Kumar, and R. R. Ravi, "Performance analysis of pre-processing filters using computed tomography images for liver lesion diagnosis", *International Journal of Biomedical Engineering and Technology* 37(2): 201–211, 2021. doi: 10.1504/ ijbet.2021.119505.

[56] S. Mishra and M. Agarwal, "Skin Cancer Classifier: Performance Enhancement Using Deep Learning Models", *10th International Conference on Signal Processing and Communication (ICSC)*, pp. 721-725, 2025. doi: 10.1109/icsc64553.2025.10969043.

[57] K. He, X. Zhang, S. Ren, and J. Sun, "Identity mappings in deep residual networks", *arXiv (Cornell University)*, 2016. doi: 10.48550/arxiv.1603.05027.

[58] S. Zagoruyko and N. Komodakis, "Wide residual networks", *arXiv (Cornell University)*, 2016. doi: 10.48550/arxiv.1605.07146.

[59] G. Huang, Z. Liu, L. Van Der Maaten, and K. Q. Weinberger, "Densely Connected Convolutional Networks", *In Proceedings of the IEEE Conference on Computer Vision and Pattern Recognition*, pp. 22612269, 2017, doi: 10.1109/cvpr.2017.243.

[60] N. Shanila, R. S. V. Kumar, and R. R. Ravi, "Segmentation of liver computed tomography images using dictionary-based snakes", *International Journal of Biomedical Engineering and Technology*, 39(3), 283–293, 2022. doi: 10.1504/ijbet. 2022. 124188.

[61] D. C. Malo, Md. M. Rahman, J. Mahbub, and M. M. Khan, "Skin Cancer Detection using Convolutional Neural Network", *IEEE 12th Annual Computing and Communication Workshop and Conference (CCWC)*, pp. 01690176, 2022, doi: 10.1109/ccwc54503. 2022.9720751.

[62] W. Yin, J. Huang, J. Chen, and Y. Ji, "A study on skin tumor classification based on dense convolutional networks with fused metadata", *Frontiers in Oncology* 12(1), 989894–989900, 2022. doi: 10.3389/fonc.2022.989894.

[63] Z. Qin, Z. Liu, P. Zhu, and Y. Xue, "A GAN-based image synthesis method for skin lesion classification", *Computer Methods and Programs in Biomedicine* 195(1): 105568–1055575, 2020. doi: 10.1016/j.cmpb.2020.105568.

[64] J. Rashid et al., "Skin cancer disease detection using transfer learning technique", *Applied Sciences*, 12(11): 5714–5723, 2022. doi: 10.3390/app12115714.

[65] A. Tafsast, M. L. Hadjili, H. Hafdaoui, A. Bouakaz, and N. Benoudjit, "Automatic Gaussian mixture model (GMM) for segmenting 18F-FDG-PET images based on Akaike information criteria", *4th International Conference on Electrical Engineering (ICEE)*, pp. 14, 2015. doi: 10.1109/intee.2015.7416845.